Nanoscale

Accepted Manuscript

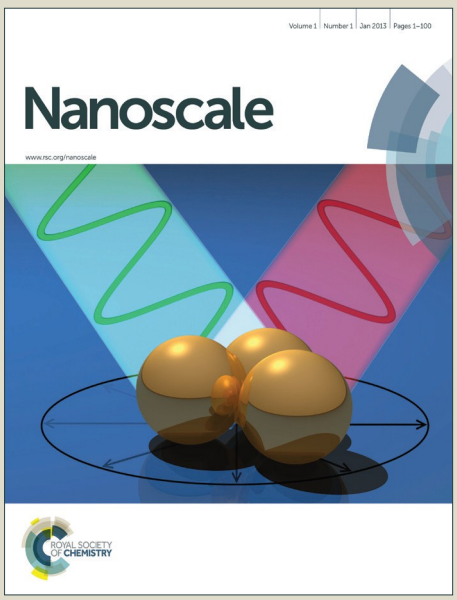

ROYAL SOCIETY OF CHEMISTRY

www.rsc.org/nanoscale

Journal Name

ARTICLE

Mussel-inspired one-pot synthesis of transition metal and nitrogen co-doped carbon (M/N-C) as efficient oxygen catalyst for Zn-air batteries

Received 00th January 20xx,
Accepted 00th January 20xx

DOI: 10.1039/x0xx00000x

www.rsc.org/

Bing Li,‡[a] Ye Chen,‡[b] Xiaoming Ge,[a] Jianwei Chai,[a] Xiao Zhang,[b] T. S. Andy Hor,[a,c] Guojun Du,[a] Zhaolin Liu,*[a] Hua Zhang *[b] and Yun Zong*[a]

Transition metal and nitrogen co-doping into carbon is an effective approach to promote the catalytic activities towards oxygen reduction reaction (ORR) and/or oxygen evolution reaction (OER) in the resultant electrocatalysts, M/N-C. The preparation of such catalysts, however, is often complicated and in low yield. Herein we report a robust approach for easy synthesis of M/N-C hybrids in high yield, which includes a mussel-inspired polymerization reaction at room temperature and a subsequent carbonization process. With the introduction of selected transition metal salts into aqueous solution of dopamine (DA), the obtained mixture self-polymerizes to form metal-containing ploydopamine (M-PDA) composites, *e.g.* Co-PDA, Ni-PDA and Fe-PDA. Upon carbonization at elevated temperature, these metal-containing composites were converted into M/N-C, *i.e.* Co-PDA-C, Ni-PDA-C and Fe-PDA-C, respectively, whose morphologies, chemical compositions, and electrochemical performances were fully studied. Enhanced ORR activities were found in all the obtained hybrids, with Co-PDA-C standing out as the most promising catalyst with excellent stability and catalytic activities towards both ORR and OER. This was further proven in Zn-air batteries (ZnABs) in terms of discharge voltage stability and cycling performance. At a discharge-charge current density of 2 mA cm^{-2} and 1 hr per cycle, the Co-PDA-C based ZnABs were able to steadily cycle up to 500 cycles with only a small broadening in the discharge-charge voltage gap which notably outperformed Pt/C; At a discharge current density of 5 mA cm^{-2}, the battery continuously discharged for more than 540 h with the discharge voltage above 1 V and a voltage drop rate of merely 0.37 mV h^{-1}. With simplicity and scalability of the synthetic approach and remarkable battery performances, the Co-PDA-C hybrid catalyst is anticipated to play an important role in practical ZnABs.

Introduction

Zn-air batteries (ZnABs) have emerged as a promising option of renewable energy techniques to meet fast increasing demand for clean energy sources and storage devices, thanks to their high energy density, good safety, environmental benignity, and the cost-advantages inherited from the abundance of zinc with easy recycling feature.[1-5] To enable a high performance ZnAB, a key component is the oxygen electrocatalyts on cathode that efficiently helps "breath-in" gaseous O_2 *via* oxygen reduction reaction (ORR) on discharging and "breath-out" it *via* oxygen evolution reaction (OER) on charging, respectively.[2,6]

Precious-metal-based catalysts are known highly efficient in electrocatalysis toward ORR,[7-10] and/or OER.[2,5,11] The prohibitive cost and scarcity,[2] however, excluded their use as catalysts in widespread or large scale applications, *e.g.* electric vehicles and grid energy storage. Considerable efforts were devoted to exploring non-precious-metal based[12-15] or metal-free catalysts,[16-25] which led to the discovery of a wide range of good catalysts, such as transition metal oxides,[13,26-29] nitrides[30], nitrogen-doped carbon (N-C)[18-20] and their hybrids,[31-39] etc.. More recently, transition metal and nitrogen co-doped carbon (M/N-C) emerged as a promising new type of catalysts, since both nanostructured metal oxides[27,29] and N-C[18-20] are known individually as efficient oxygen electrocatalysts. Their hybrids, *i.e.* M/N-C, exhibited comparable or even superior catalytic activity and durability to precious metal-based catalysts,[37] benefitted from carbon-metal interaction induced synergetic effect.[37,38,40] Started by Dai et al. with N-doped graphene (N-

[a] Institute of Materials Research and Engineering (IMRE), A*STAR (Agency for Science, Technology and Research), 2 Fusionopolis Way, Innovis #08-03, Singapore 138634, Republic of Singapore. E-mail: zl-liu@imre.a-star.edu.sg; y-zong@imre.a-star.edu.sg.

[b] Center for Programmable Materials, School of Materials Science and Engineering, Nanyang Technological University, 50 Nanyang Avenue, Singapore 639798, Republic of Singapore. E-mail: hzhang@ntu.edu.sg.

[c] Department of Chemistry, National University of Singapore, 3 Science Drive 3, Singapore 117543, Republic of Singapore

† Electronic Supplementary Information (ESI) available: Schematic structure of ZnAB; photos of home-made of ZnABs; EDX spectra and elemental mapping of M-PDA-C; N_2 adsorption/desorption isotherms, high magnification TEM images of M-PDA-C, and RDE data of M-PDA-C, etc. See DOI: 10.1039/b000000x

‡ These authors contributed equally to this work

G)[18] and N-doped carbon nanotubes (N-CNTs)[19] that efficiently promoted ORR, follow-up studies revealed that growing Co_3O_4 nanoparticles (NPs) on N-CNTs or N-G boosted the bifunctional catalytic performance of either individuals.[37,38] With the similar phenomenon observed in other materials' systems[35,38,41,42] it is reasonable to assume synergetic effect as a common key to enable more powerful oxygen catalysts.

Compared to post-growth of active NPs on pre-synthesized N-CNTs or N-G, a more straightforward route to M/N-C is the direct conversion of metal and N-containing compounds[33,43] or composites[13,15,44,45] *via* high temperature thermal treatments. With carbon and nitrogen sources from the organic/polymeric segments, the metal species are transformed into catalytically active nanoparticles at high temperature and firmly attached onto N-C to form M/N-C concurrently. Such process represents a robust and scalable approach for mass production of M/N-C.

Dopamine (DA), a N-containing molecule, is responsible for the extremely firm adhesion of invertebrate mussels to diverse surfaces.[46] DA readily self-polymerizes at room temperature to form polydopamine (PDA) films on virtually any solid surfaces, which has been proven useful in both bio-[47-49] and non-bio[50-54] applications. More than an N-doping agent, DA also possesses reduction power and contains chelating –OH groups which can "capture" metal ions during polymerization to form metal/PDA composites (M-PDA) as desirable precursors of M/N-C. A few recent reports have shown M/N-C hybrids as efficient oxygen catalysts.[35,42,55,56] Li and co-workers synthesized Co/N-C under solvothermal condition followed by carbonization;[35] Lu *et al*. obtained Fe/N-C from pre-synthesized PDA spheres of sub-micrometer mediated by aqueous ammonia;[56] Fe/N-C hollow spheres were prepared using SiO_2 nanospheres as templates, with subsequent carbonization and KOH etching.[42] All these methods use autoclaves and/or sacrificial templates with some additional steps and chemicals, which notably compromised their utility and feasibility in cost-sensitive applications, *e.g.* in ZnABs for electric vehicles and grid energy storage. In addition, the absence of battery tests data leaves unanswered questions with regard to their stability and suitability for ZnABs,[4,17,36] as the corrosion power of a typical 6 M KOH aqueous electrolyte in practical ZnABs is much stronger than that of the 0.1 M KOH used in electrochemical studies. A facile and scalable method to produce cost-effective M/N-C hybrids, supported by well-understood performances in Zn-Air batteries, is clearly in demand.

Herein, we report such a method to produce M-PDA-C (M = Fe, Co, or Ni) hybrids. Essentially, M-PDA-C was obtained by carbonizing the respective precursor M-PDA, synthesized *via* a simple and robust one-pot reaction in an aqueous solution at room temperature without any special equipment or sacrificial templates. Electrochemical studies revealed Co-PDA-C as the most ORR active species, with its OER activity superior to that of Pt/C. Ni-PDA-C showed excellent OER but modest ORR activity, while Fe-DPA-C was found inferior in both ORR and OER catalytic performance. ZnABs using Co-PDA-C in the air-cathode exhibited outstanding battery performance in terms of high and stable discharge voltage and long cycling stability.

Experimental

Synthesis of PDA carbon (PDA-C)

PDA was synthesized by simply polymerizing DA in 10 mM of Tris(hydroxymethyl)aminomethane (Tris) buffer solution (pH = 8.5) at room temperature. Typically, DA was added into Tris buffer solution while gently stirring to reach a concentration of 1 mg/mL. The solution turned pink within a few minutes and then dark-brown after 24 h. The product PDA was collected via centrifugation, washed by deionized (DI) water for three times, and freeze-dried. Carbonization process was carried out by heating PDA in N_2 atmosphere at a heating rate of 5 °C min^{-1} to 900 °C and maintained at the temperature for 30 min. The final carbonized product was denoted by PDA-C.

Synthesis of M-PDA-C hybrids

The synthesis of M-PDA-C hybrids followed a similar procedure as PDA-C, except the addition of a selected metal salt during DA polymerization. Typically, 400 mg DA was added to 400 mL Tris solution (pH=8.5) while gently stirring. After 20 min of reaction, 5 mL of 10 mM $M(NO_3)_n$ (n=2 for M = Co, Ni; and n=3 for M = Fe) aqueous solution was introduced to the reaction mixture. M-PDA was collected *via* centrifugation after 24 h of reaction, washed by DI water for three times and then freeze-dried. Carbonizing M-PDA at 900 °C led to the formation of final product, denoted by M-PDA-C.

Characterizations

A Field Emission Scanning Electron Microscope (FE-SEM, JSM-7600F) and a Transmission Electron Microscope (TEM, Philips CM300) were used to visualize the morphologies of M-PDA-C. Energy dispersive X–ray (EDX) spectra and elemental mapping were captured by an EDS detector (Oxford INCA) equipped on the SEM. X-ray diffraction (XRD) patterns were recorded with a Bruker D2 Phaser using Cu K_α radiation source. N_2 adsorption and desorption isotherms were measured using Automated Surface Area and Pore Size Analyzer of Quadrasorb SI (Quantachrome Instruments), from which the specific surface area, pore size and its distributions were determined following Brunauer-Emmett-Teller (BET) and Battett-Joyner-Halenda (BJH) methods.[17] X–ray photoelectron spectroscopy (XPS) data was collected from a Theta Probe electron spectrometer (VG ESCALAB200i–XL, Thermo Scientific).

Electrochemical measurements

Cyclic voltammetry (CV) and linear sweep voltammetry (LSV) measurement was performed on an Autolab potentiostat/ galvanostat (PGSTAT302N) station combined with a rotating disk electrode (RDE) using 0.1 M KOH electrolyte pre-purged by O_2 or N_2. Pt foil and Ag/AgCl electrode (saturated with 3 M KCl) were employed as the counter and reference electrodes, respectively. For standardization, the reference was calibrated and converted to reversible hydrogen electrode (RHE) using the equation of E (RHE) = E (Ag/AgCl) + 0.059pH + 0.197.[7] To prepare the working electrode, 5 mg of active material was dispersed in 1 mL aqueous solution of Nafion (1 wt.%, diluted from 5 wt.% water solution, Sigma Aldrich), and sonicated for ~ 30 min to form a homogeneous catalyst ink. Aliquots of such

ink was carefully dropped onto a glassy carbon electrode (GC, 5 mm in diameter) and dried in fume hood under ambient condition. The catalyst loading was 0.5 mg cm^{-2} for PDA-C and M-PDA-C hybrids, and 0.12 mg cm^{-2} for Pt/C (20 wt.% of platinum on carbon black).

The number (*n*) of electrons transferred per O_2 molecule in ORR was calculated using Koutecky-Levich (K-L) equations as follows:

$$\frac{1}{j} = \frac{1}{j_L} + \frac{1}{j_K} = \frac{1}{B\omega^{1/2}} + \frac{1}{j_K} \quad (1)$$

$$B = 0.2nFC_0D_0^{2/3}\nu^{-1/6} \quad (2)$$

$$j_K = nFkC_0 \quad (3)$$

where *j* is the measured current density, j_K and j_L are the kinetic limiting and diffusion limiting current densities, respectively; ω is the angular velocity, *F* is Faraday constant, C_0 is the bulk concentration of O_2, D_0 is the diffusion coefficient of O_2, *v* is the kinematic viscosity of the electrolyte and *k* is the electron-transfer rate constant.[15,37]

ZnAB assembly and tests

ZnABs were assembled with home-built Zn-air cells (Fig. S1, ESI†) and evaluated using galvanostatic method on a battery tester (NEWARE BTS-610). All discharge and discharge-charge tests were conducted at room temperature under ambient open air condition. 6 M KOH aqueous solution containing 0.2 M $ZnCl_2$ (to facilitate charging process) was used as the electrolyte with polished zinc plate as the anode. The air cathodes using hybrid material of Co-PDA-C or commercial Pt/C as catalysts with a loading density of ~ 1.0 mg cm^{-2} were prepared following a previously reported method.[15]

Results and Discussion

Phase structure of the obtained hybrids was characterized by X-ray diffraction (XRD), and the results are presented in Fig. 1. The typical (002) peak of carbonaceous materials are seen for all three samples, confirming successful conversion of PDA into carbon by carbonization at 900°C. In addition, 3 well-defined peaks are observed for Co-PDA-C and Ni-PDA-C hybrids which match well to (111), (200) and (220) planes of face-centred cubic (*fcc*) cobalt (JCPDS No. 15-0806) and nickel (JCPDS No. 04-0850), implying the metallic nature of Co or Ni species in the respective M-PDA-C sample. In contrast, the XRD pattern of Fe-PDA-C is somehow complicated. Fe_3C, a composition commonly presents in high temperature pyrolysis product of Fe/N-containing organic composites,[56,57] was found (peaks marked with asterisks in Fig. 1) to co-exist with the metallic Fe. EDS analysis suggests the compositions of M-PDA-C hybrids as carbon and metals, with the metal species evenly distributed across the entire sample according to the elemental mapping results (Fig. S2, ESI†).

Detailed structural and morphological information of the M-DPA-C hybrids were obtained from SEM and TEM images. As shown in Fig. 2, Co-PDA-C comprises numerous carbon

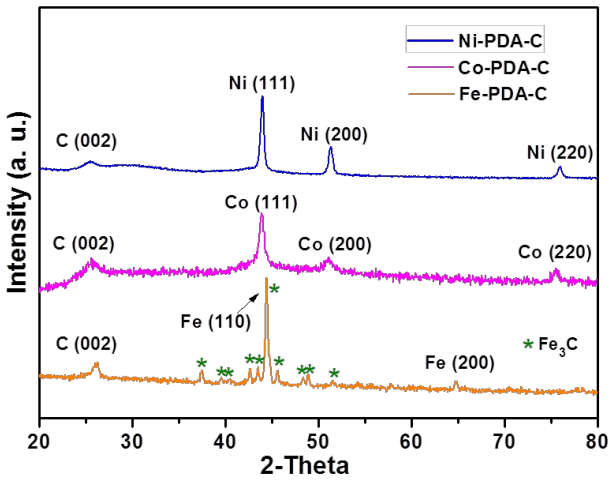

Fig. 1 XRD patterns of Ni-PDA-C (blue line), Co-PDA-C (pink line) and Fe-PDA-C (orange line), respectively, suggesting metallic feature of Ni and Co NPs in their respective hybrids, and the co-existence of Fe_3C and metallic Fe NPs in Fe-PDA-C.

particles of irregular shapes but a similar size (~ 200 nm) which coalesced to form a continuous porous carbon matrix. Within the matrix are homogeneously distributed Co NPs of 10 to 35 nm in diameter (Fig. 2A and E). Such structure of small Co NPs embedded in a porous carbon matrix provides high population of active sites and large interfaces, enabling fast transfer of electrons in electrochemical reactions. Moreover, the surrounding carbons kept Co NPs apart from each other thus effectively mitigated the agglomeration issues, offering high catalytic stability to the catalyst. Such morphology is similar to that of the recently reported Co-PDA-C hybrids synthesized using solvothermal method[35] which exhibited high catalytic activities towards both ORR and OER. Obviously, the facile method herein is of notable advantages.

In the Ni-PDA-C hybrid, smaller carbon particles formed the carbon matrix (Fig. 2B and F), and Ni NPs are found bigger with noticeably reduced loading density. The 3rd hybrid, Fe-PDA-C, appeared as a matrix of film/sheet-like carbons with even bigger and polydispersed Fe NPs at further reduced loading density (Fig. 2C and G). Nevertheless, in the absence of metal ions, PDA-C was obtained as monodispersed spherical particles with a size of about 200 nm (Fig. 2D and H), which are similar to PDA-C spheres synthesized *via* ammonia-mediated method in a mixture solvent of ethanol and DI water.[56] The noticeable variation in the morphology with the introduction of transition metal ions are likely due to the strong coordination reaction between the metal ions and PDA, which notably changed the behaviours of PDA in the fomration of polymer micelles thus the morphology of the finally dried and carbonized samples.

The surface area and pore size distribution of the M-PDA-C hybrids were determined from nitrogen adsorption-desorption isotherms (Fig. S3, ESI†). The obtained BET specific surface areas are in the order of Ni-PDA-C > Co-PDA-C > Fe-PDA-C with their value being 368.4, 276.1 and 113.3 $m^2\ g^{-1}$, respectively, which is in consistence with their respective morphologies observed in SEM and TEM images. The relatively low BET

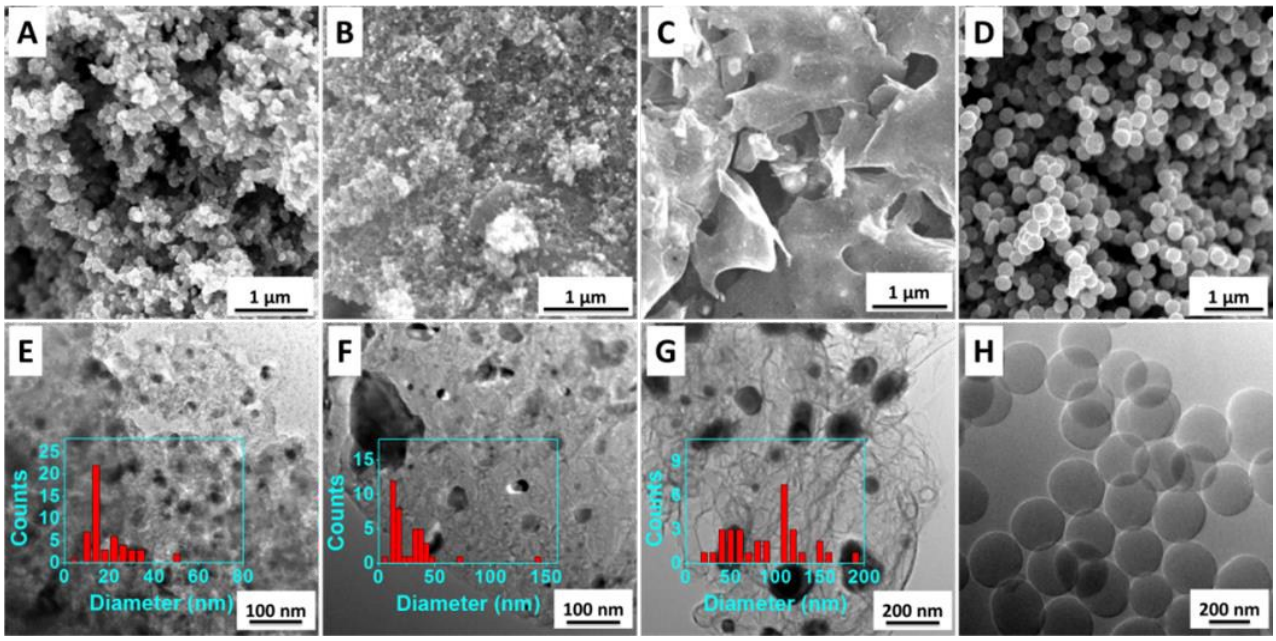

Fig. 2 A-D) SEM images showing the morphologies of Co-PDA-C (A), Ni-PDA-C (B), Fe-PDA-C (C) and PDA-C (D). E-H) the corresponding TEM images of Co-PDA-C (E), Ni-PDA-C (F), Fe-PDA-C (G) and PDA-C (H). The insets in (E-G) illustrating the size distributions of the corresponding metal NPs of the samples.

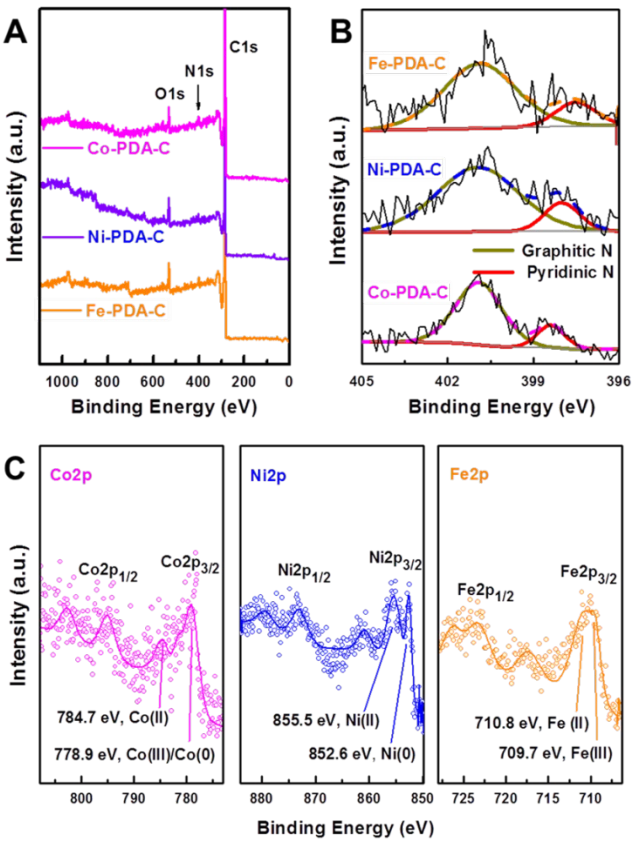

Fig. 3 XPS spectra of the Ni-PDA-C, Co-PDA-C and Fe-PDA-C hybrids. A) Survey scans. B) High-resolution spectra of N 1s. C) High-resolution spectra of Ni 2p, Co 2p and Fe 2p.

specific surface area of Fe-PDA-C hybrids, the bigger particle size and lower loading density of Fe/FeC_3 imply significantly reduced effective active sites and interface areas as compared to those of Co-PDA-C and Ni-PDA-C hybrids, imposing clear disadvantages to the sample in electrochemical performances.

The chemical states of the hybrids were investigated by XPS with the survey spectra shown in Fig. 3A. The strong C1s peaks observed are in good agreement with the EDS analysis, suggesting carbon as the major element in M-PDA-C hybrids. The high-resolution N1s spectra confirmed successful doping of N into the carbon matrices. Two predominant N deduced from the N1s spectra are graphitic N at 401.3 eV and pyridinic N at 398.6 eV (Fig. 3B), in agreement with early reports of the dopamine derived N-doped carbons.[56] Both graphitic N and pyridinic N are known to promote ORR activity notably.[35,42,58]

The high-resolution Ni 2p, Co 2p and Fe 2p spectra (Fig. 3C) are obtained for the 3 hybrids as anticipated; however, unlike the strong signals of metallic (zero valence state) NPs observed in XRD, obvious oxidation states can be found in the respective XPS spectra.[35,59] The difference is likely attributed to the highly surface sensitive feature of XPS which typically probes a depth of less than 10 nm from sample surface. Therefore, the most of 2P signals could have come from the metal NPs close to the sample surfaces which are prone to oxidation. The majority of the NPs embedded inside the carbon matrix, however, are believed to remain in their metallic form as suggested by XRD data. Even for NPs which are close to the sample edges, their surfaces are covered by carbon layers with thickness of a few nm (Fig. S4, ESI†), moving them out of the focus of XPS beam. Hence, it is not difficult to understand the much lower intensities of 2p signals in XPS (Fig. 3A and C), which makes a sharp contrast to the high density of NPs observed in SEM (Fig. 2A-C) and TEM (Fig. 2E-G) as well as the strong diffraction peaks for elemental metals in XRD (Fig. 1).

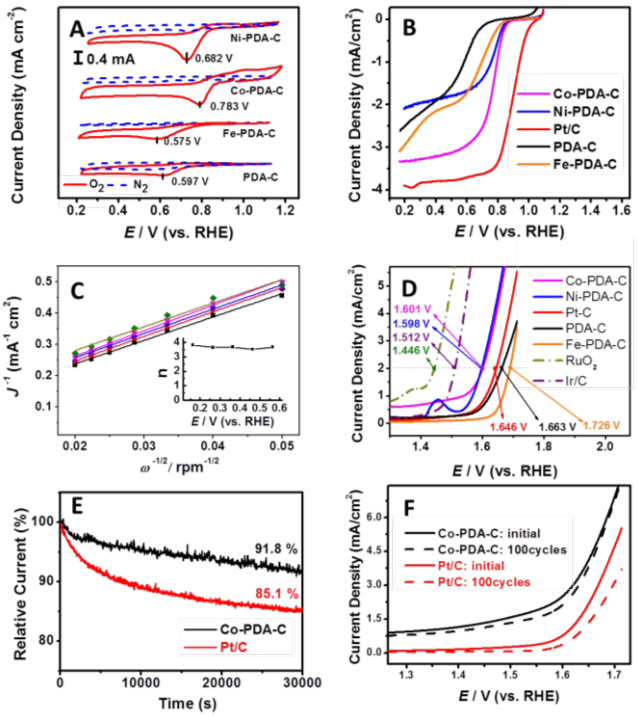

Fig. 4 Electrochemical data of the hybrids: A) CV curves in O_2- (red solid lines) and N_2-purged (blue dashed lines) in 0.1 M KOH. B) LSV curves of the hybrids and PDA-C compared with Pt/C for ORR at a rotating speed of 900 rpm. C) The K-L plots and fitting curves of Co-PDA-C derived from its RDE data (Fig. S5B, ESI†) between the potentials from 0.564 to 0.164 V. Inset: plot of the electron transfer number (n) per oxygen molecule (O_2) at different potentials. D) LSV curves of the hybrids and PDA-C compared with Pt/C, RuO_2 and Ir/C for OER. E) *i-t* plots of Co-PDA-C and Pt/C at 0.564 V in O_2-satruated 0.1 M KOH at an electrode rotating speed of 400 rpm. F) ADT results of Co-PDA-C (black) and Pt/C (red) before (solid lines) and after 100 cycles (dashed lines) at electrode rotating speed of 400 rpm for OER. The scan rate was kept at 10 mV s^{-1} for CVs and 5 mV s^{-1} for RDE and ADT measurements.

To evaluate the electrochemical performance of M-PDA-C hybrids, CV, LSV and RDE measurements were performed in 0.1 M KOH, with PDA-C and benchmark ORR catalyst of Pt/C being taken as the control samples and tested under the same conditions. In CV measurements, the cathodic peaks observed at 0.783 (Co-PDA-C), 0.682 (Ni-PDA-C), 0.575 (Fe-PDA-C) and 0.597 V (PDA-C) in the presence of O_2 proved ORR activities of all 4 samples (Fig. 4A). The more positively shifted ORR peak for Co-PDA-C implies its higher activity towards ORR. In order to facilitate a better comparison, RDE measurements were carried out at various rotating rates in O_2-saturated 0.1 M KOH (Fig. S5, ESI†) The LSV curves of the 3 hybrids, metal-free PDA-C, and commercial Pt/C at a rotating rate of 900 rpm are plotted together in Fig. 4B. Apparently, all the three M-PDA-C hybrids exhibited notably improved catalytic activity towards ORR as compared to PDA-C, the metal-free carbon nanospheres. Co-PDA-C, again, demonstrated the highest ORR catalytic activity, as evidenced by its highest current density among the 4 at any given potential and more positively shifted LSV curve. The half-wave potential ($E_{1/2}$) of about 767 mV (*vs* RHE) for Co-PDA-C was only 95 mV more negative than that of Pt/C ($E_{1/2}$: 862 mV), but notably more positive as compared to that of Ni-PDA-C ($E_{1/2}$: 722 mV), Fe-PDA-C ($E_{1/2}$: 629 mV) and PDA-C ($E_{1/2}$: 546 mV). Moreover, the current density of Co-PDA-C at $E_{1/2}$ was also much higher. Therefore, the ORR activity of the M-PDA-C hybrids and PDA-C are determined in the order of Co-PDA-C > Ni-PDA-C > Fe-PDA-C > PDA-C.

The low ORR activity of Fe-PDA-C obtained in this work notably differs from those reported Fe and N co-doped carbon (Fe-N-C) of high ORR activities,[32,42,55-57,60,61] although they may contain virtually similar chemical species. It is worth noting that the exact role of Fe in Fe-N-C electrocatalysts for oxygen reduction is still under debate.[32,42,55-57,60] Some researchers proposed FeN_x, FeC_3 and Fe_3O_4 as the species providing the ORR active sites,[42,55,56,60] whereas research of others showed no change of ORR activity after the removal of Fe from Fe–N–C by harsh treatments (HF or hot H_2SO_4 leaching).[32,61] It has been noted that the one common feature shared by those excellent ORR electrocatalysts of Fe-N-C was the large BET specific surface areas, typically about 700 to 1500 m^2 g^{-1}.[32,42,61] As the less ORR active Fe-PDA-C obtained in this work possesses a relative limited BET specific surface area of 113.3 m^2 g^{-1}, it seems to imply that its low ORR activity could be ascribed, at least partially, to the much lower BET specific surface area which notably reduced number of active sites and interfaces for ORR. Nevertheless, one cannot completely exclude other factors which may affect ORR performance of Fe-PDA-C, e.g. configuration and content of doped N, graphitic degree of carbon and Fe/Fe_3C nanoparticle size and surface states, etc.. In-depth understanding on the relationship between the ORR performance and the intrinsic properties of Fe-PDA-C will be the key to further advance the development of such catalyst.

The ORR catalytic activity of Co-PDA-C was further studied using K-L plots (Fig. 4C) derived from its RDE curves (Fig. S5B, ESI†) in the voltage range of 0.564 to 0.164 V. The good linearity and parallelism can be clearly seen from the plots, revealing the first-order kinetics of ORR against the concentration of dissolved O_2.[15,37] The number (n) of electrons transferred per oxygen molecule (O_2) was calculated to be 3.5-3.8, suggesting that Co-PDA-C promoted ORR in desirable 4-electron transfer dominated process. In contrast, Ni-PDA-C and Fe-PDA-C are believed to catalyze ORR *via* a 2-electron or a mixed 4- and 2-electron pathway according to the calculated results (Fig. S5E and F, ESI†), whereby the involvement of 2-electron transfer process leads to generation of detrimental peroxide species.

The OER catalytic activity of M-PDA-C and PDA-C was also investigated, and the results are shown in their LSV curves in Fig. 4D. Clearly, Co-PDA-C hybrid showed descent OER activity by less positive potential as compared to that of Pt/C, Fe-PDA-C and PDA-C at any given current density, but notably lower than that of the state-of-art OER catalyst of noble metal-based RuO_2 and Ir/C. For instance, at a current density of 2 mA cm^{-2} the potential of 1.601 V for Co-PDA-C is about 45, 62 and 89 mV less positive than that of Pt/C, PDA-C and Fe-PDA-C, respectively. This value is merely 3 mV more positive than that of Ni-PDA-C, the best OER catalyst in this work, but 155 and 89 mV more positive than that of RuO_2 and Ir/C, respectively. The

trend of OER activity change among all these samples can be more clearly observed from their d*i*/d*V* curves (Fig. S6, ESI†). Nevertheless, in concentrated potassium hydroxide needed for ZnABs both RuO_2 and Ir/C presented durability issues (inferior to Co-PDA-C, will be discussed in the next paragraphs), and the non-precious metal feature and easy preparation in large scale still give Co-PDA-C the competitive advantages in applications with high volume needs of batteries.

Long-term stability is another crucial factor for the practical applications of rechargeable ZnABs. Accordingly, the durability of Co-PDA-C in ORR and OER was assessed by recording the chronoamperometric (*i* - *t*) data and conducting accelerated degradation tests (ADT), respectively, with Pt/C taken as the benchmark. As shown in the *i* – *t* response (Fig. 4E), Co-PDA-C exhibited high durability for ORR with 91.8% retention of its initial current density after 30,000 s of continuous operation; whereas Pt/C suffered a rapid loss of the voltammetric current with a current retention of 85.1% under the same experiment conditions. ADT results shown in Fig. 4F (black lines) further confirmed the excellent durability and stability of Co-PDA-C towards OER, as its LSV curve saw little changes after 100 continuous cycles. In contrast, clear degradation was observed in the OER performance of Pt/C (Fig. 4F, red lines), RuO_2 and Ir/C (Fig. S7, ESI†) after 100 cycles of operation under the same conditions. These electrochemical data have unveiled Co-PDA-C as a desirable electrocatalyst with pronounced activities and good durability for both ORR and OER, making it a promising bifunctional catalyst for rechargeable Zn-air batteries.

The performance of ZnAB with Co-PDA-C as catalyst in air cathode was evaluated in home-built cells, using commercially available catalysts of Pt/C, Ir/C and RuO_2 as the control for comparison purposes. Galvanostatic discharge-charge cycling tests were conducted at a current density of 2 mA cm^{-2}, with 30 minutes discharge followed by 30 minutes charge in each cycle. The cycling performances of ZnABs constructed using different catalysts are presented in Fig. 5A and B (detailed comparisons summarized in Table S1, ESI†), and the advantage of ZnAB with Co-PDA-C based air-cathode can be seen clearly. Compared to its Pt/C based counterpart, it initially required a higher charge voltage (2.15 *vs* 2.03 V) and delivered a slightly lower discharge voltage (1.21 *vs* 1.27 V); however, it caught up in 6 cycles for discharge and 10 cycles for charge, respectively. Compared to ZnABs with Ir/C or RuO_2-based air cathode, Co-PDA-C based ZnABs delivered a similar initial discharge voltage (1.21 *vs* 1.21 and 1.20 V for Ir/C and RuO_2), but more stable in cycling tests over a slightly longer period (at 60th cycle, 1.24 *vs* 1.20 and 1.04 V for Ir/C and RuO_2). Despite lower initial charge voltages, ZnABs with Ir/C or RuO_2 catalyst suffered quick drop in discharge voltages, which rapidly widened their voltage gaps (inversely proportional to the energy efficiency of batteries) and made them lose their competitive advantages to Co-PDA-C based ZnABs in merely about 53 and 40 cycles (Fig. S8, ESI†). For cycling over even longer period, as shown in Fig. 5A-C, Co-PDA-C based ZnAB worked robustly over 500 cycles (or 500 h) with merely an increase of 0.03 V in the charge voltage (2.15 to 2.18 V, 0.06 mV/cycle). With a total drop of 0.20 V in the discharge voltage (1.21 to 1.01 V, 0.40 mV/cycle) the overall increment in the discharge-charge voltage gap was 0.23 V (0.46 mV/cycle). In sharp contrast Pt/C, Ir/C or RuO_2 based ZnABs deteriorated much faster, showing as faster widening of the voltage gap between charge and discharge potential over the cycling tests (Fig. 5A and Fig. S8, ESI†). Take Pt/C as an example, after 60 cycles (or 60 h) the charge voltage drastically increased from its initial value of 2.03 V to the cut-off voltage of 2.4 V (0.37 V, 6.2 mV/cycle). With a drop of 0.12 V in discharge voltage (1.27 to 1.15 V, 2.0 mV/cycle) it has led to a notably enlarged discharge-charge voltage gap of 0.49 V (8.2 mV/cycle) at the end of cycling test. With a degradation rate of 5 times in discharge voltage (2.0 *vs* 0.4 mV/cycle) and over 100 times in charge voltage (6.2 *vs* 0.06 mV/cycle), the charge-discharge voltage gap of Pt/C based ZnAB widened 18 times as fast as that of its Co-PDA-C based counterpart. The unanimous and unambiguous data from the cycling tests in ZnABs further proved Co-PDA-C as an efficient and highly stable bifunctional oxygen electrocatalyst. The fast worsening of the performance of batteries using precious metal based catalysts, according to a very recent report,[62] is due to the use of the carbon support with low degree of crystallinity which is more easily etched by strong alkaline electrolyte. Hence, the protection provided by carbons of graphitic layered structure in our catalysts should be one of the main origins of the improved cycling stability.

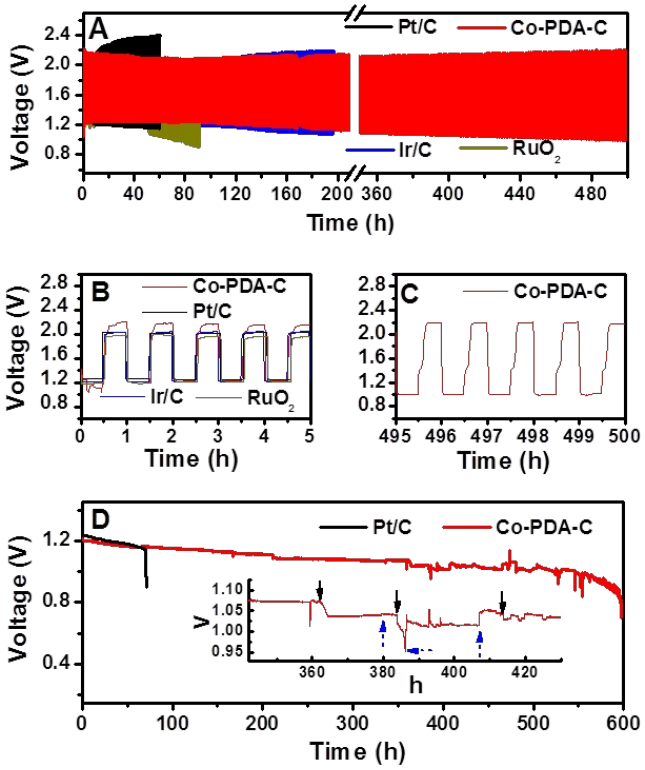

Fig. 5 A) Discharge-charge cycling performances of ZnABs based on Co-PDA-C (red), Pt/C (black), Ir/C (blue) and RuO_2 (green) at 2 mA cm^{-2}. B and C) selected cycles from A) to show the details. D) Voltage profile of a Co-PDA-C based ZnAB compared with a Pt/C based ZnAB when fully discharged at a current density of 5 mA cm^{-2}, the inset shows the details of selected period of the Co-PDA-C based ZnAB(from 340-430 h).

Fig. 5D presents typical galvanostatic discharge profiles at a constant current density of 5 mA cm^{-2} for Co-PDA-C based ZnAB, which is compared with its counterpart using the state-of-art ORR catalyst, Pt/C. Clearly, ZnAB with Pt/C catalyst degraded much faster despite a higher initial discharge voltage (1.24 *vs* 1.20 V for Co-PDA-C based ZnABs), in good agreement with the good ORR activity but poor stability of Pt/C according to the electrochemical studies. Remarkably, the Co-PDA-C based ZnAB was able to discharge continuously over an ultra-long period of 600 h (25 full days and nights) with a characteristic flat voltage plateau at above 1.0 V for about 540 h (more than 3 weeks) and a slow degradation rate of 0.37 mV h^{-1}. The specific capacity, as normalized to the consumed Zn by weighing the difference of the Zinc plate before and after the long-term discharge test, was estimated to be 658 mAh g^{-1} which outperformed recently reported ZnAB using N-doped meso/micro porous carbon catalyst[22] and was comparable to other top performers.[6,17,63] The high specific capacity and flat discharge plateau with very slow voltage drop rate over an extended operation period without changing the electrolyte or Zn anode[23] are convincing features arising from outstanding ORR catalytic activity and excellent durability of Co-PDA-C. The outstanding performance of resultant ZnAB is in consistence with its decent electrocatalytic activities and stability shown above, suggesting great potential of Co-PDA-C in rechargeable Zn-air batteries.

It is worth noting that the noises appeared after 350 h in the discharge curve in Fig. 5D were associated with electrolyte leakage, whereby electrolyte droplets were observed to form at air cathode (Fig. S9, ESI†). These droplets partially blocked the air pathway and in turn reduced the air/oxygen supply, leading to sudden voltage drop (black arrows in the inset in Fig. 5D). The voltage profile can be recovered to a certain extent (blue dashed arrows in the inset in Fig. 5D), once the droplets fell off or were removed manually from the air cathode. Such phenomenon of air cathode blockage and electrolyte shortage caused voltage drop has been verified by control experiments (Fig. S10, ESI†, and also see the supplementary video 1 and 2). In general, leakage issue is getting worse after a prolonged period of operation (*e.g.*, over 400 h in the test shown in Fig. 5D) due to corrosion of carbon paper, which eventually leads to the termination of battery operation by electrolyte leakage and/or possible detachment of the catalyst. Severe corrosion into the carbon paper support made of fibers of low crystalline carbons has also been clearly evidenced by the notably reduced mechanical strength of the catalytic air-cathode and the obvious colour changes of the electrolyte in the tested ZnAB (supplementary video 3 and Fig. S11, ESI†) Effective solutions to help mitigate electrolyte leakage are hence essential to the further improvement of ZnAB life time, which may include the development of alkaline corrosion-resistant air-cathode of high electric conductivity and high mechanical strength, plus good bifunctional catalytic activities and high stability. For instance, metal foam or mesh with high mechanical strength might be employed to replace the conventionally used carbon paper as current collector, with a persistent hydrophobic backing layer or superhydrophobic coatings on air cathode, etc. which are currently being explored in our lab.

Conclusions

In summary, a series of M/N-C hybrids have been synthesized by simply introducing metal ions into aqueous solutions of self-polymerizable dopamine, followed by a post carbonization of the resultant metal-polydopamine composites, M-PDA. The metal ions were found to play a critical role in the structure and morphology of the resultant M-PDA-C hybrids. In details, the hybrid with Co^{2+} appeared as a porous matrix of coalesced carbon particles with embedded small metallic Co NPs; for Ni^{2+} the porous matrix was made of smaller carbon particles and filled by bigger and fewer metallic Ni NPs; whereas the use of Fe^{3+} led to bulky sheet-like carbon matrix with much larger and polydispersed Fe/FeC_3 NPs; in the absence of metal ions, only monodispersed PDA-C NPs formed with a size of *ca.* 200 nm. Electrochemical studies revealed the enhanced ORR activity of M-PDA-C hybrids as compared to the metal-free PDA-C. The Co-PDA-C stood out as the best ORR catalyst among the three M-PDA-C hybrids by more positive half-wave potential, higher current density and pseudo 4-electron transfer behaviour in ORR. Concurrently, it outperformed Pt/C in OER activity and durability towards ORR and OER. The excellent electrochemical properties of Co-PDA-C were further confirmed in prototype ZnABs, by the retention of discharge voltage above 1 V for over 540 h at 5 mA cm^{-2} without changing electrolyte and/or Zn anode, or steadily cycling over 500 cycles at 2 mA cm^{-2} with only a small increase of 0.23 V in the discharge-charge voltage gap. These results have demonstrated Co-PDA-C hybrid as a competitive candidate of efficient yet low-cost and scalable oxygen catalyst for ZnAB batteries.

The current work highlights convenient incorporation of non-precious transition metal into mussel-inspired PDA at room temperature without any additional mediating chemicals or sophisticated apparatus, which are of distinct advantages towards mass production of M/N-C hybrids in a cost effective and environmentally friendly way. The success demonstrated in this work is shedding a light on the development of M/N-C hybrids for ZnAB industries and other catalyst-critical industrial applications.

Acknowledgements

This research was conducted under the project of IMRE/12-2P0504, which is part of Advanced Energy Storage Research Programme supported by Science and Engineering Research Council (SERC) of A*STAR (Agency for Science, Technology and Research), Singapore. H.Z. thanks the support from MOE under AcRF Tier 2 (ARC 26/13, No. MOE2013-T2-1-034; ARC 19/15, No. MOE2014-T2-2-093) and AcRF Tier 1 (RGT18/13, RG5/13), and NTU under Start-Up Grant (M4081296.070.500000) in Singapore. This Research is also conducted by NTU-HUJ-BGU Nanomaterials for Energy and Water Management Programme

under the Campus for Research Excellence and Technological Enterprise (CREATE), that is supported by the National Research Foundation, Prime Minister's Office, Singapore.

Notes and references

1 J.-S. Lee, S. T. Kim, R. Cao, N.-S. Choi, M. Liu, K. T. Lee and J. Cho, *Adv. Energy Mater.*, 2011, **1**, 34-50.
2 F. Cheng and J. Chen, *Chem. Soc. Rev.*, 2012, **41**, 2172-2192.
3 Z.-L. Wang, D. Xu, J.-J. Xu and X.-B. Zhang, *Chem. Soc. Rev.*, 2014, **43**, 7746-7786.
4 P. Pei, K. Wang and Z. Ma, *Appl. Energy*, 2014, **128**, 315-324.
5 Y. Li and H. Dai, *Chem. Soc. Rev.*, 2014, **43**, 5257-5275.
6 Y. Li, M. Gong, Y. Liang, J. Feng, J.-E. Kim, H. Wang, G. Hong, B. Zhang and H. Dai, *Nat. Commun.*, 2013, **4**, 1805.
7 A. Holewinski, J.-C. Idrobo and S. Linic, *Nat. Chem.*, 2014, **6**, 828-834.
8 C. Zhu and S. Dong, *Nanoscale*, 2013, **5**, 10765-10775.
9 D. Zhang, C. Zhang, D. Mu, B. Wu and F. Wu, *Acta Chim. Sinica*, 2013, **71**, 1101-1110.
10 A. Morozan, B. Jousselme and S. Palacin, *Energy Environ. Sci.*, 2011, **4**, 1238-1254.
11 Y.-C. Lu, Z. Xu, H. A. Gasteiger, S. Chen, K. Hamad-Schifferli and Y. Shao-Horn, *J. Am. Chem. Soc.*, 2010, **132**, 12170-12171.
12 R. Cao, J. S. Lee, M. L. Liu and J. Cho, *Adv. Energy Mater.*, 2012, **2**, 816-829.
13 W. T. Hong, M. Risch, K. A. Stoerzinger, A. Grimaud, J. Suntivich and Y. Shao-Horn, *Energy Environ. Sci.*, 2015, **8**, 1404-1427.
14 X. Ge, Y. Liu, F. W. T. Goh, T. S. A. Hor, Y. Zong, P. Xiao, Z. Zhang, S. H. Lim, B. Li, X. Wang and Z. Liu, *ACS Appl. Mater. Interfaces*, 2014, **6**, 12684-12691.
15 B. Li, X. Ge, F. W. T. Goh, T. S. A. Hor, D. Geng, G. Du, Z. Liu, J. Zhang, X. Liu and Y. Zong, *Nanoscale*, 2015, **7**, 1830-1838.
16 L. Dai, Y. Xue, L. Qu, H.-J. Choi and J.-B. Baek, *Chem. Rev.*, 2015, **115**, 4823-4892.
17 B. Li, D. Geng, X. S. Lee, X. Ge, J. Chai, Z. Wang, J. Zhang, Z. Liu, T. S. A. Hor and Y. Zong, *Chem. Commun.*, 2015, **51**, 8841-8844.
18 L. Qu, Y. Liu, J.-B. Baek and L. Dai, *ACS Nano*, 2010, **4**, 1321-1326.
19 K. Gong, F. Du, Z. Xia, M. Durstock and L. Dai, *Science*, 2009, **323**, 760-764.
20 Y. Li, W. Zhou, H. Wang, L. Xie, Y. Liang, F. Wei, J.-C. Idrobo, S. J. Pennycook and H. Dai, *Nat. Nanotechnol.*, 2012, **7**, 394-400.
21 L. Chen, R. Du, J. Zhu, Y. Mao, C. Xue, N. Zhang, Y. Hou, J. Zhang and T. Yi, *Small*, 2015, **11**, 1423-1429.
22 H.-W. Liang, X. Zhuang, S. Brüller, X. Feng and K. Müllen, *Nat. Commun.*, 2014, **5**, 4973.
23 J. Zhang, Z. Zhao, Z. Xia and L. Dai, *Nat. Nanotechnol.*, 2015, **10**, 444-452.
24 D. Geng, N. Ding, T. S. A. Hor, Z. Liu, X. Sun and Y. Zong, *J. Mater. Chem. A*, 2015, **3**, 1795-1810.
25 J. Zhang, Z. Xia and L. Dai, *Sci. Adv.*, 2015, **1**, e1500564.
26 S. Liu, L. Hu, X. Xu, A. A. Al-Ghamdi and X. Fang, *Small*, 2015, **11**, 4267-4283.
27 P. W. Menezes, A. Indra, D. González-Flores, N. R. Sahraie, I. Zaharieva, M. Schwarze, P. Strasser, H. Dau and M. Driess, *ACS Catal.*, 2015, **5**, 2017-2027.
28 C. Wei, L. Yu, C. Cui, J. D. Lin, C. Wei, N. Mathews, F. Huo, T. Sritharan and Z. Xu, *Chem. Commun.*, 2014, **50**, 7885-7888.
29 F. Cheng, J. Shen, B. Peng, Y. Pan, Z. Tao and J. Chen, *Nat. Chem.*, 2011, **3**, 79-84.
30 Y. Jia, y. wang, L. Dong, J. Huang, Y. Zhang, J. Su and J. Zang, *Chem. Commun.*, 2015, **51**, 2625-2628.
31 Y. Jiang, Y. Lu, X. Wang, Y. Bao, W. Chen and L. Niu, *Nanoscale*, 2014, **6**, 15066-15072.
32 W. Niu, L. Li, X. Liu, N. Wang, J. Liu, W. Zhou, Z. Tang and S. Chen, *J. Am. Chem. Soc.*, 2015, **137**, 5555-5562.
33 W. Xia, R. Zou, L. An, D. Xia and S. Guo, *Energy Environ. Sci.*, 2015, **8**, 568-576.
34 R. Zhang, S. He, Y. Lu and W. Chen, *J. Mater. Chem. A*, 2015, **3**, 3559-3567.
35 Y. Su, Y. Zhu, H. Jiang, J. Shen, X. Yang, W. Zou, J. Chen and C. Li, *Nanoscale*, 2014, **6**, 15080-15089.
36 J.-S. Lee, G. S. Park, H. I. Lee, S. T. Kim, R. Cao, M. Liu and J. Cho, *Nano Lett.*, 2011, **11**, 5362-5366.
37 Y. Liang, Y. Li, H. Wang, J. Zhou, J. Wang, T. Regier and H. Dai, *Nat. Mater.*, 2011, **10**, 780-786.
38 Y. Liang, Y. Li, H. Wang and H. Dai, *J. Am. Chem. Soc.*, 2013, **135**, 2013-2036.
39 D. U. Lee, B. J. Kim and Z. Chen, *J. Mater. Chem. A*, 2013, **1**, 4754-4762.
40 G. Zhang, B. Y. Xia, X. Wang and X. W. Lou, *Adv. Mater.*, 2014, **26**, 2408-2412.
41 K. Chen, X. Huang, C. Wan and H. Liu, *Chem. Commun.*, 2015, **51**, 7891-7894.
42 D. Zhou, L. Yang, L. Yu, J. Kong, X. Yao, W. Liu, Z. Xu and X. Lu, *Nanoscale*, 2015, **7**, 1501-1509.
43 A. Aijaz, N. Fujiwara and Q. Xu, *J. Am. Chem. Soc.*, 2014, **136**, 6790–6793.
44 P. Song, Y. Zhang, J. Pan, L. Zhuang and W. Xu, *Chem. Commun.*, 2015, **51**, 1972-1975.
45 C. Zhu, J. Zhai and S. Dong, *Chem. Commun.*, 2012, **48**, 9367-9369.
46 H. Lee, S. M. Dellatore, W. M. Miller and P. B. Messersmith, *Science*, 2007, **318**, 426-430.
47 J. H. Waite and X. X. Qin, *Biochemistry*, 2001, **40**, 2887-2893.
48 J. Ryu, S. H. Ku, H. Lee and C. B. Park, *Adv. Funct. Mater.*, 2010, **20**, 2132-2139.
49 Y. Liu, L. Lu and K. Ai, *Chem. Rev.*, 2014, **114**, 5057–5115.
50 L. Yang, J. Kong, D. Zhou, J. M. Ang, S. L. Phua, W. A. Yee, H. Liu, Y. Huang and X. Lu, *Chem. Eur. J.*, 2014, **20**, 7776-7783.
51 S. Xiong, Y. Wang, J. Zhu, J. Yu and Z. Hu, *Langmuir*, 2015, **31**, 5504-5512.
52 M. J. Harrington, A. Masic, N. Holten-Andersen, J. H. Waite and P. Fratzl, *Science*, 2010, **328**, 216-220.
53 Y. Wei, J. Kong, L. Yang, L. Ke, H. R. Tan, H. Liu, Y. Huang, X. W. Sun, X. Lu and H. Du, *J. Mater. Chem. A*, 2013, **1**, 5045-5052.
54 X. Yao, C. Zhao, J. Kong, D. Zhou and X. Lu, *RSC Adv.*, 2014, **4**, 37928-37933.
55 J. Xiao, J. Xi, Y. Xia, y. Xu and S. Wang, *Chem. Commun.*, 2015, **51**, 10479-10482.
56 K. Ai, Y. Lu, C. Ruan, L. Lu and G. Lu, *Adv. Mater.*, 2013, **25**, 998-1003.
57 M. Xiao, J. Zhu, L. Feng, C. Liu and W. Xing, *Adv. Mater.*, 2015, **27**, 2521-2527.
58 L. F. Lai, J. R. Potts, D. Zhan, L. Wang, C. K. Poh, C. H. Tang, H. Gong, Z. X. Shen, L. Y. Jianyi and R. S. Ruoff, *Energy Environ. Sci.*, 2012, **5**, 7936-7942.
59 X. Lu and C. Zhao, *Nat. Commun.*, 2015, **6**, 6616.
60 J. Liu, X. Sun, P. Song, Y. Zhang, W. Xing, W. Xu, *Adv. Mater.,* 2013, **25**, 6879-6883.
61 D. S. Yang, M. Y. Song, K. P. Singh, J. S. Yu, *Chem. Commun.,* 2015, **51**, 2450-2453.
62 A. Zadick, L. Dubau, N. Sergent, G. Berthomé, M. Chatenet, *ACS Catal.*, 2015, **5**, 4819-4824.
63 M. Prabu, K. Ketpang and S. Shanmugam, *Nanoscale*, 2014, **6**, 3173-3181.